LBL-28284
Preprint

Lawrence Berkeley Laboratory
UNIVERSITY OF CALIFORNIA

Materials & Chemical Sciences Division

Submitted to Physical Review Letters

Observation of Quantum Susceptance in Superconducting Tunnel Junctions

Q. Hu, C.A. Mears, P.L. Richards, and F.L. Lloyd

December 1989

Prepared for the U.S. Department of Energy under Contract Number DE-AC03-76SF00098.

DISCLAIMER

LBL-28284

Observation of quantum susceptance in superconducting tunnel junctions

Qing Hu,[a] C.A. Mears, P.L. Richards

Department of Physics, University of California,

and Materials and Chemical Sciences Division

Lawrence Berkeley Laboratory, Berkeley, California 94720

and

F.L. Lloyd[b]

Electromagnetic Technology Division

National Institute of Standards and Technology, Boulder, Colorado 80303

Abstract

We have made the first direct measurement of the quantum susceptance which arises from the reactive part of quasiparticle tunneling in a superconductor-insulator-superconductor junction. The junction is coupled to an antenna and a superconducting microstrip stub to form a resonator; the resonant frequency is measured from the response of the junction to broadband radiation from a Fourier transform spectrometer. A 19% shift of the resonant frequency, from 73 GHz to 87 GHz, is observed that arises from the change of the quantum susceptance of the junction with dc bias voltage. The measured shift is in excellent agreement with Werthamer-Tucker theory, which includes the quantum susceptance. This quantum susceptance should exist in other tunnel devices such as quantum well structures whose nonlinear I-V characteristics are due to elastic tunneling.

PACS numbers: 74.30. Gn, 74.50. +r, 84.40. -x, 85.25. -j

a) Present address: Department of Electrical Engineering and Computer Science and Research Laboratory of Electronics, Massachusetts Institute of Technology, Cambridge, MA 02139.

b) Present address: Department of Electrical Engineering, University of Virginia, Charlottesville, Virginia 22901.

Superconductor-Insulator-Superconductor (SIS) junctions carry tunneling currents due both to Cooper pairs from the superconducting ground state and to quasiparticles excited from the ground state. The tunneling current for each type exhibits both resistive (in-phase) and reactive (out-of-phase) response to an ac drive. These two components are related through a Kramers-Kronig transform as is required for any causal linear response. For Cooper pair tunneling, the in-phase component is the Josephson $\cos\phi$ term,[1,2] while the out-of-phase component is the Josephson $\sin\phi$ term.[1,2] For quasiparticles, the quantum expression for the in-phase component depends only on the dc quasiparticle I-V characteristic, while the out-of-phase component is the so-called quantum susceptance or quantum reactance.[1-3] The reactive quasiparticle tunneling current is a result of virtual photon-assisted-tunneling. The quasiparticles slosh back and forth between the two sides of the SIS junction by absorbing and emitting virtual photons.[4]

While both phases of Josephson tunneling and quasiparticle resistive tunneling have been studied extensively, the quantum susceptance has been largely ignored. The contribution from the quantum susceptance to the tunneling current is only significant at frequencies $\hbar\omega/e \geq \Delta V$, where ΔV is the voltage range of nonlinearity.[3] Available junctions with well defined quasiparticle I-V curves generally have too much shunt capacitance to permit direct measurement at such high frequencies. Quantitative investigations of the performance of SIS quasiparticle direct detectors and mixers have raised questions about the importance of the quantum susceptance. As in the case for the Josephson $\cos\phi$ term,[5] however, the effect of the quantum susceptance is subtle even at frequencies comparable to the gap frequency. The argument has been made[6] that it would be very difficult to distinguish the effect of quantum susceptance from other effects. In this letter, we report a direct experimental measurement of the quantum susceptance of an SIS junction. This measurement is based on a measurement of the bias dependence of the resonant frequency of a circuit which contains the SIS junction. This shift of the resonant frequency is due to the change of the quantum susceptance with the dc bias voltage across the junction.

At frequencies $\hbar\omega/e > \Delta V$, where ΔV is the voltage range of the nonlinearity near the sum gap, the response of SIS junctions must be treated quantum mechanically.[3] In the small signal limit, the induced RF current I_ω and the RF voltage V_ω are related through an admittance $Y(\omega)$ which is a function of frequency due to the non-local current-voltage relation. The real (dissipative) part of $Y(\omega)$, which we call the quantum conductance $G_Q(\omega)$, is given by,[3]

$$G_Q(\omega) = \mathrm{Re}[Y(\omega)] = \frac{e}{2\hbar\omega}[I_{dc}(V_o + \hbar\omega/e) - I_{dc}(V_o - \hbar\omega/e)] \,. \qquad (1)$$

Here $I_{dc}(V_o)$ is the dc quasiparticle I-V characteristic. This characteristic can be conveniently obtained from a measurement such as the one shown in Fig. 1(a). In Eq. (1), $G_Q(\omega)$ reduces to the classical limit dI/dV at low frequencies, and approaches the inverse of the normal resistance $1/R_n$ at frequencies far above the gap frequency. The response of an SIS junction is like a classical diode at low frequencies, and becomes Ohmic when the photon energy is much greater than the gap energy. Experimental evidence for this quantum conductance has been well established and it has been utilized in SIS quasiparticle direct detection.[7]

The quantum susceptance $B_Q(\omega)$, which is the imaginary part of $Y(\omega)$, should be related to $G_Q(\omega)$ through a Kramers-Kronig transform, as is required for any causal, linear response,[8]

$$B_Q(\omega) = \mathrm{Im}[Y(\omega)] = P\int_{-\infty}^{+\infty} \frac{d\omega'}{\pi} \frac{G_Q(\omega')}{\omega' - \omega} \,, \qquad (2)$$

where P stands for principle value. From Eq. (2), we can show that the quantum susceptance $B_Q(\omega)$ can be expressed as,

$$B_Q(\omega) = \frac{e}{2\hbar\omega}[I_{KK}(V_o + \hbar\omega/e) - 2I_{KK}(V_o) + I_{KK}(V_o - \hbar\omega/e)] \,. \qquad (3)$$

Where $I_{KK}(V)$ is the real part of the quasiparticle response function at frequency $\omega = e(V-V_o)/\hbar$.[1-3] It can be expressed as a voltage Kramers-Kronig transform of $I_{dc}(V)$,

$$I_{KK}(V) = P\int_{-\infty}^{+\infty} \frac{dV'}{\pi} \frac{I_{dc}(V') - V'/R_n}{V' - V} \quad . \tag{4}$$

An example of I_{KK} is shown in Fig. 1(b). The result (3) was derived previously[9] from Tucker's theory[3] by expanding the local oscillator-induced current to first order in V_ω. According to this theory, the measured quasiparticle dc I-V curve $I_{dc}(V_o)$ contains all the information about the high frequency response of the quasiparticles in an SIS junction, provided that only elastic tunneling contributes to $I_{dc}(V_o)$.

Equation (3) has a very clear geometric meaning: $B_Q(\omega)$ is a measure of the curvature of the three points $I_{KK}(V_o + \hbar\omega/e)$, $I_{KK}(V_o)$, and $I_{KK}(V_o - \hbar\omega/e)$. When the curvature is upward, the quantum susceptance B_Q is positive; when the curvature is downward, the quantum susceptance is negative. It can be seen from Fig. 1(b) that as we increase the dc bias voltage V_o from zero, the curvature changes from positive to negative and back to positive. This implies that the quantum susceptance changes from capacitive to inductive and back to capacitive as is shown in Fig. 1(d). Note that B_Q has the largest capacitive value at one photon voltage $\hbar\omega/e$ below the sum gap voltage V_g because the curvature has the largest positive value at this point. B_Q has the largest inductive value at V_g because the curvature has the largest negative value at this point. The physical explanation of the voltage dependence of B_Q will be discussed based on a model of a two-level system in a forthcoming paper.[10] In Fig. 1(c), we also plot the quantum conductance G_Q as a function of bias voltage. There is a well defined maximum in G_Q over the voltage range for which a quasiparticle can tunnel by absorbing or emitting one photon.

We have measured the voltage dependence of the quantum susceptance by observing the voltage dependent shift of the resonant frequency of a circuit consisting of an SIS junction and a superconducting microstrip stub. The resonator is excited by the chopped output of a far-

infrared Fourier transform spectrometer (FTS) which is coupled using a planar lithographed antenna. The excitation level of the circuit is obtained from the chopped component of the dc current of the junction, which is operated as an SIS direct detector.[7] A picture and a schematic drawing of the SIS junction with the microstrip stub located at the center of a log-periodic antenna are shown in Fig. 2(a) and (b). The response of this resonator to a small RF signal can be analyzed by using the equivalent circuit shown in Fig. 2(c). The signal source is represented by an RF current source in parallel with the real antenna admittance Y_A. The SIS junction is represented by the parallel combination of the quantum conductance $G_Q(\omega)$, quantum susceptance $B_Q(\omega)$, and the geometric capacitance C. The superconducting microstrip stub is assumed to be lossless and is represented by a susceptance $B_{stub}(\omega)$. The imbedding susceptance B_{IMB}, which is defined as the total susceptance that is independent of dc bias voltage, is just the sum of the susceptances of the junction capacitance ωC and of the microstrip stub $B_{stub}(\omega)$. The resonance of the equivalent circuit of Fig. 2(c) corresponds to the condition $B_{total} = B_Q(\omega) + B_{IMB}(\omega) \doteq 0$. Without the quantum susceptance B_Q, the resonant frequency ω_0 would be independent of bias voltage. Since B_Q changes rapidly with dc bias voltage V_0 as shown in Fig. 1(d), however, we expect that ω_0 will change as V_0 is changed.

Each part of this experiment was designed to minimize the effect of standing wave resonances which could distort the measurement, especially at bias voltages above $V_g - \hbar\omega_0/e$ where the resonant Q is low. An FTS was used as a signal source, rather than a coherent microwave oscillator because the poor spatial coherence helps to average over standing waves. A very broadband antenna design was used. The stub design was chosen to minimize the frequency dependence of the stub susceptance. The use of the internal detection mechanism in the SIS junction avoids the possibility of standing waves that can arise in the coupling to an external detector.

The apparatus used in this experiment is essentially the same as was used in our quasioptical SIS mixer experiments.[11] The output of the step-and-integrate FTS is connected to the cyrostat through a 11-mm diameter light pipe. Inside the cryostat, the signal beam is

focused by a f/0.85 TPX lens, and then by a hyperhemispherical quartz lens to a f/0.5 converging beam. The log-periodic antenna is centered on the flat side of the hyperhemispherical quartz lens. The quartz lens is heat sunk to the 4.2 K liquid helium through a copper support.

Examples of the measured detector output ΔI_{dc} as a function of the path difference of the FTS are shown in Figs. 3(a) and (b). Figures 3(c) and (d) show the spectral response of the circuit obtained by averaging 5 to 10 Fourier transforms of such interferograms and correcting for the spectrometer efficiency. Figures 3(a) and (c) were measured with $V_0 = 2.350$ mV which is far enough below V_g that the resonance peak is narrow and not fully resolved. Figures 3(b) and (d) are for $V_0 = 2.500$ mV, where the resonance peak is wide due to the large value of quantum conductance G_Q seen in Fig. 1(c) and is essentially fully resolved. The interferogram (b) has been truncated so as to filter out fringes which arise from standing waves in the quasioptical system.

Since the antenna-coupled SIS direct detector sees only a single electromagnetic mode, the spectral intensity of the output of the FTS is the frequency independent Rayleigh-Jeans spectrum multiplied by the frequency dependent beamsplitter efficiency.[12] After normalizing these spectra over the beamsplitter efficiency, we obtain the resonant frequencies by least-mean-square fitting the top half of the resonance peaks to 2nd to 4th order polynomials. The degree of the polynomials required in the fitting is determined by the asymmetry of the peak. The estimates of possible errors in the measured resonant frequencies are chosen as the frequency ranges over which the fitted polynomials have more than 90% of their peak values. The result is plotted in Fig. 4(a) as a function of dc bias voltage. Below 2.150 mV and above 2.650 mV, the signal/noise ratio of the spectra is too poor to obtain reliable information on the resonant frequencies. The error bars are larger for $V_0 > 2.450$ mV where the peaks are broad. The measured resonant frequencies clearly show a smooth shift as the dc bias voltage changes. The most dramatic change of the resonant frequency takes place in the voltage range from

2.400 to 2.650 mV, where the quantum susceptance B_Q changes rapidly from capacitive to inductive.

A quantitative comparison of the measured bias dependent frequency shift of our circuit with theory requires a precise evaluation of all circuit parameters. The log-periodic antenna[13] used in this experiment has a real and frequency-independent admittance,[14] $Y_A = ((1+\varepsilon)/2)^{1/2}/189\ \Omega^{-1}$. For quartz substrates, $\varepsilon = 3.85$, so $Y_A = 8.3\times10^{-3}\ \Omega^{-1}$. The SIS junction is a $Nb/Al_2O_3/Nb$ sandwich made using the tri-layer process.[15] Its I-V curve in Fig. 1(a) shows a low leakage current and a sharp gap structure even at the estimated temperature of 4.5 K. The junction area is estimated to be $2.5\times2.5\ \mu m^2$, which gives a geometric capacitance of 0.28 pF if we assume a specific capacitance value of 45 $fF/\mu m^2$.[16]

The microstrip stub shown in Figures 2(a) and (b) is made out of Pb-In-Au alloy that is separated from the Nb ground plane by a layer of insulating SiO. The stub consists of a narrow section (1) with width $w_1 = 6\ \mu m$ and length $l_1 = 135\ \mu m$ and a wide section (2) with $w_2 = 40\ \mu m$ and $l_2 = 260\ \mu m$. The phase velocity in the microstrip line is $v = 1/(L_S C_S)^{1/2}$, where $L_S = (\mu_o/kw)[t + \lambda_1 \coth(t_1/\lambda_1) + \lambda_2 \coth(t_2/\lambda_2)]$ is the inductance per unit length,[17] and $C_S = k\varepsilon_r\varepsilon_o w/t$ is the capacitance per unit length.[17] Here t and ε_r are the thickness and the relative dielectric constant of the insulating layer of SiO, $t_{1,2}$ and $\lambda_{1,2}$ are the thicknesses and the London penetration depths of the ground (Nb) and top (Pb-In-Au) planes, and k is a fringing factor that is close to unity. Using the designed values, $\varepsilon_r = 5.7$,[18] $t = 3000$ Å, $t_1 = 2000$ Å, $t_2 = 4250$ Å, $\lambda_{Nb} = 850$ Å,[18] $\lambda_{Pb\text{-}In\text{-}Au} = 1450$ Å,[18] the phase velocity is $v = 0.30\pm0.01$ c. The length of the wider section is $\lambda/4$ at 87 GHz, so this section transforms an RF open circuit at point A to an RF short circuit at point B.[19] This design gives a slower variation of the susceptance as a function of frequency than that for an open-ended stub.[20] The length of the narrow section is $\lambda/8$ at 85 GHz which transforms the RF short to an inductive admittance. The total susceptance of the two-section stub is given by[19]

$$B_{stub} = \frac{Y_1[Y_2 \tan(\beta l_2) + Y_1 \tan(\beta l_1)]}{Y_1 - Y_2 \tan(\beta l_1) \tan(\beta l_2)} \quad , \tag{5}$$

where $\beta = \omega/v$, and the characteristic admittances $Y = (C_S/L_S)^{1/2}$ of the narrow and wide sections of the stub are $Y_1 = 0.124\ \Omega^{-1}$, and $Y_2 = 0.637\ \Omega^{-1}$ respectively. The induced dc current per unit available RF power P_A at the antenna terminals as a function of RF frequency is given by,

$$\frac{\Delta I_{dc}}{P_A} = S_I(\omega) \left[1 - \left|\frac{Y_A - Y_J^*}{Y_A + Y_J}\right|^2\right] \quad . \tag{6}$$

Where $Y_J = G_Q + i(B_Q + \omega C + B_{stub})$ is the total admittance of the SIS junction and the stub. The current responsivity $S_I(\omega)$ of the SIS direct detector is given by[3]

$$S_I(\omega) = \frac{\Delta I_{dc}}{P_\omega} = \frac{e}{\hbar\omega} \frac{I_{dc}(V_o + \hbar\omega/e) - 2I_{dc}(V_o) + I_{dc}(V_o - \hbar\omega/e)}{I_{dc}(V_o + \hbar\omega/e) - I_{dc}(V_o - \hbar\omega/e)} \quad , \tag{7}$$

where $P_\omega = I_\omega V_\omega/2$ is the coupled RF power. Because the reactive quasiparticle response function I_{KK} does not appear in Eq. (7) the quantum susceptance does not affect this responsivity. Since $S_I(\omega)$ is a smooth function of frequency, except at $e(V_g - V_o)/\hbar$, the frequency which corresponds to the maximum ΔI_{dc} is mainly determined by the resonance condition of the circuit, $Im(Y_J) = B_Q + \omega C + B_{stub} = 0$.

In order to make an accurate comparison between theory and experiment, we calculated theoretical estimates of the detector output and analyzed them by the same procedures used for the experimental data. First, we computed the induced dc current as a function of RF frequency using Eq. (6). Second, we convolved these computed spectra with the Fourier transform of the apodization function which was used for the experimental interferograms.[21] The calculated results (dashed lines) are compared with the experimental results (solid lines) in Fig. 3(c) for

V_0 = 2.350 mV and 3(d) for V_0 = 2.500 mV. The calculation reproduces most important features of the data. For example, the shoulder on the high frequency side of (c) arises from the frequency dependence in Eq. (7). Third, we fitted the same number of computed data points at the same discrete frequencies with the same order of polynomials as we did from the experimental data. The theoretically calculated curve of the resonant frequency as a function of V_0 is shown in Fig. 4(a) as the solid line. It is in excellent agreement with the experimental result. As a comparison, the dashed line, which is essentially flat and obviously differs from the experimental results, is the voltage dependence of the peak frequency of the resonance without the quantum susceptance B_Q. The weak voltage dependence of the dashed line is due to the change of the current responsivity $S_I(\omega)$ in Eq. (7) with the bias voltage V_0. Clearly, the experimental results provide decisive evidence for the quantum susceptance.

We would like to emphasize that the values of two key parameters, the junction capacitance C = 0.275 pF, and the phase velocity v = 0.286 c, which were used in our theoretical computation, are essentially the same as the ones we estimate from the geometric dimensions, 0.28 pF and 0.30±0.01 c. As a check on these parameters, we have measured the resonant frequency at 0.158 mV where the responsivity of the junction contains a sharp peak that arises from the nonlinear interaction of the Josephson oscillation with the resonant circuit.[10] The quantum susceptance B_Q from Fig. 1(d) is negligible at this low bias voltage. The measured resonant frequency of 77 GHz coincides with the dashed line in Fig. 4(a), which is the theoretical prediction for B_Q = 0. This essentially perfect agreement verifies the values of C and v which were used in our theoretical calculations.

As a further check on the circuit parameters used in our theoretical simulation, we have independently deduced values of C = 0.275 pF and v = 0.272 c by fitting pumped I-V curves using the method published previously.[9] The small differences between these two estimates correspond to an overall vertical shift of the solid theoretical line in Fig. 4(a) by about 3 GHz.[10]

We also investigated the possibility that Josephson response has an effect on the shift of the resonant frequency by applying a magnetic field to change the Josephson critical current. We did not see any change of the resonant frequency within our experimental accuracy up to a field corresponding to several magnetic flux quanta in the junction. This is not surprising since in our bias voltage range (2.15 - 2.65 mV), the Josephson current oscillates at frequencies above 1 THz, which are effectively shunted by the capacitance.

In Fig. 4(b), we plot the 3-dB linewidths Δf of the resonance peaks as a function of the bias voltage. The experimental values of Δf were obtained from the best fit polynomials. The solid line is the calculated one. Again, the agreement between experiment and the theory is excellent. The sharp increase of Δf at 2.45 mV corresponds to the sharp increase of the quantum conductance G_Q at one photon voltage $\hbar\omega/e$ below the gap voltage V_g. Note from Fig. 1(d) that the quantum susceptance has the largest capacitive value at this voltage, $V_g - \hbar\omega/e$, so the resonant frequency is the lowest as shown in Fig. 4(a). There is some disagreement between the theoretical and experimental values of Δf near $V_0 = 2.5$ mV. This discrepancy arises because the experiment probes the region of the I-V curve around $V_0 + \hbar\omega/e$ which lies just above the sum gap voltage. Like most Nb-based junctions, our junction has a negative resistance in this region due to the proximity effect which is not correctly reproduced by our measurement system.

In conclusion, we have made the first direct measurement of the quantum susceptance by measuring the shift of the resonant frequency of a resonator which contains an SIS junction. The observed shift, from 73 GHz to 87 GHz, and the excellent agreement with Werthamer-Tucker theory, is clear evidence of the existence of the quantum susceptance. Our result has therefore, directly verified one of the important aspects of the above theory. This aspect, the existence of a reactive component which is associated with a nonlinear tunneling I-V characteristic, should apply to other tunnel devices such as the quantum well structures.[22] The nonlinear dc I-V curves of those devices are due to elastic tunneling, so their RF admittance $Y(\omega)$ is given by Eqs. (1) and (3) which can be obtained entirely from their dc I-V curves.

We would like to thank D. Miller and W.N. Creager for assisting with the FTS experiment, and J.E. Carlstrom for lending us a 60-90 GHz Gunn oscillator. We would also like to thank M.J. Feldman, M.J. Wengler, and S. Feng for helpful discussions. This work was supported in part by the Director, Office of Energy Research, Office of Basic Energy Sciences, Materials Sciences Division of the U.S. Department of Energy under Contract No. DE-AC03-76-SF00098, and by the Department of Defense.

References

1. N.R. Werthamer, Phys. Rev. **147**, 255 (1966).
2. R.E. Harris, Phys. Rev. **B11**, 3329 (1975).
3. J.R. Tucker, IEEE J. Quantum Electronics, **QE-15**, 1234 (1979); J.R. Tucker and M.J. Feldman, Rev. Mod. Phys. **57**, 1055 (1985).
4. E. Yablonovitch, J.P. Heritage, D.E. Aspnes, and Y. Yafet, Phys. Rev. Lett. **63**, 976 (1989).
5. See for example, O.H. Soerensen, J. Mygind, and N.F. Pedersen, Phys. Rev. Lett. **39**, 1018 (1977), and the references therein.
6. M.J. Feldman, J. Appl. Phys. **53**, 584 (1982).
7. P.L. Richards, T.-M. Shen, R.E. Harris, and F.L. Lloyd, Appl. Phys. Lett. **36**, 480 (1980).
8. J.D. Jackson, **Classical Electrodynamics**, chapter 7, 2nd Edition, John Wiley & Sons, New York, (1975).
9. C.A. Mears, Q. Hu, and P.L. Richards, IEEE Trans. **MAG-25**, 1050 (1989).
10. Q. Hu, C.A. Mears, P.L. Richards, and F.L. Lloyd, to be submitted to Phys. Rev. **B**, (1990).
11. Q. Hu, C.A. Mears, P.L. Richards, and F.L. Lloyd, IEEE Trans. **MAG-25**, 1380 (1989).
12. Q. Hu, C.A. Mears, P.L. Richards, and F.L. Lloyd, Int. J. Infrared and Mm Waves, **9**, 303 (1988).
13. P.H. Siegel, IEEE Microwave Theory Tech. **MTT-S Digest**, 649 (1986).
14. D.B. Rutledge, D.P. Neikirk, and D.P. Kasilingam, in **Infrared and Millimeter Waves**, ed. K.J. Button, pp. 1-90, Academic Press, New York, (1983).
15. M. Gurvitch, M.A. Washington, and H.A. Huggins, Appl. Phys. Lett. **42**, 472 (1983).

16. A.W. Lichtenberger, C.P. McClay, R.J. Mattauch, M.J. Feldman, S.-K. Pan, and A.R. Kerr, IEEE Trans. **MAG-25**, 1247 (1989); S. Han, J. Lapointe, and J.E. Lukens, Phys. Rev. Lett. **63**, 1712 (1989).

17. W.H. Chang, J. Appl. Phys. **50**, 8129 (1979).

18. J.H. Greiner et al. IBM J. Res. Dev. **24**, 195 (1980).

19. R.E. Collin, **Foundations for microwave engineering**, chapter 5. McGraw-Hill, New York, (1966).

20. A.R. Kerr, S.-K. Pan, and M.J. Feldman, Int. J. Infrared and Mm Waves, **9**, 203 (1988).

21. R.J. Bell, **Introductory Fourier Transform Spectroscopy**, Chapter 5, Academic Press, New York, (1972).

22. L.L. Chang, L. Esaki, and R. Tsu, Appl. Phys. Lett. **24**, 593 (1974); T.C.L.G. Sollner, W.D. Goodhue, P.E. Tannenwald, C.D. Parker, and D.D. Peck, Appl. Phys. Lett. **43**, 588 (1983); M. Tsuchiya, T. Matsusue, and H. Sakaki, Phys. Rev. Lett. **59**, 2359 (1987).

Figure Captions

Figure 1. (a) Measured dc I-V curve at T ~ 4.5 K of the $Nb/Al_2O_3/Nb$ SIS junction studied in this letter. (b) Kramers-Kronig transform of I_{dc} calculated using Eq. (4). (c) Quantum conductance G_Q at $\omega/2\pi$ = 77 GHz calculated from Eq. (1) using the $I_{dc}(V_o)$ in Fig. 1(a). (d) Quantum susceptance B_Q at 77 GHz calculated from Eq. (3) using the $I_{KK}(V_o)$ in Fig. 1(b).

Figure 2. (a) Photograph of a log-periodic antenna with a microstrip stub, the SIS junction is located at one end of the stub and at the center of the antenna. (b) Schematic of a two-section microstrip stub. The open circuit at point A is transformed to a short circuit at point B by the $\lambda/4$ stub. (c) Equivalent circuit of a resonator which includes a microstrip stub B_{stub}, a junction capacitance C, the quantum susceptance B_Q, and the quantum conductance G_Q. Both B_Q and G_Q are functions of dc bias voltage. The radiation source and the antenna are represented with an RF current source in parallel with the antenna admittance Y_A.

Figure 3. Interferograms measured with a Fourier transform spectrometer, (a) at V_o = 2.35 mV, (b) at V_o = 2.50 mV. Spectra after correcting for beamsplitter efficiency corresponding to the above interferograms, (c) at 2.35 mV, (d) at 2.50 mV. The dashed lines in (c) and (d) are the computed spectra.

Figure 4. (a) Resonant frequency as a function of dc bias voltage. The dots are the experimentally measured results; the solid line is calculated theoretically; the dashed line is the calculated result without including the quantum susceptance. Note the dashed line is essentially flat vs. V_o. (b) Linewidth of the resonance as a function of V. The dots are the experimental results and the solid line is calculated. $\omega_o/2\pi$ = 77 GHz is the resonant frequency of the imbedding susceptance without the quantum susceptance B_Q.

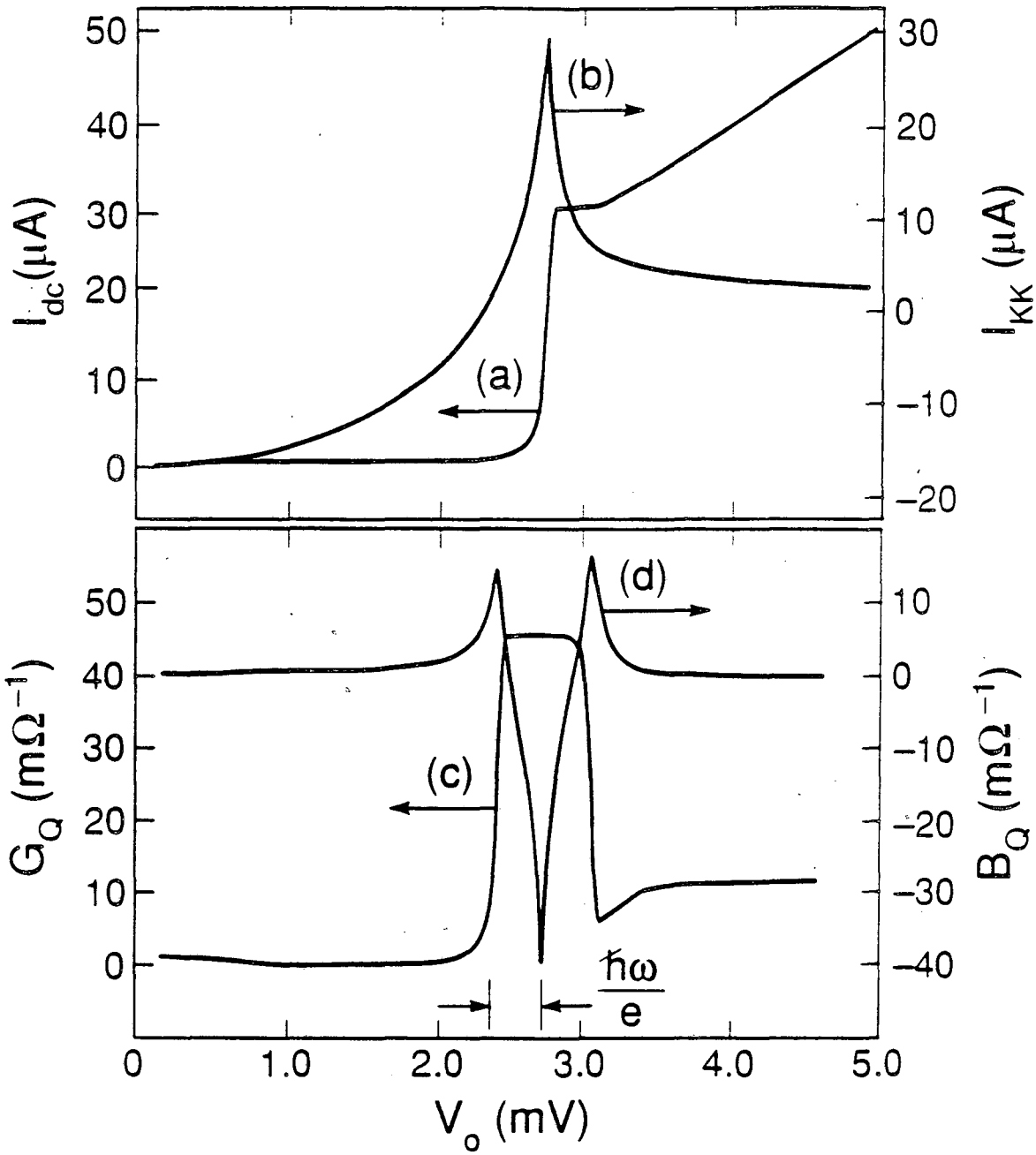
50
40
30
20
10
0
30
20
10
0
−10
−20
(b)
(a)
I_{dc}(μA)
I_{KK} (μA)
50
40
30
20
10
0
10
0
−10
−20
−30
−40
(d)
(c)
G_Q (mΩ^{-1})
B_Q (mΩ^{-1})
ħω/e
0
1.0
2.0
3.0
4.0
5.0
V_o (mV)

Figure 1

(a)

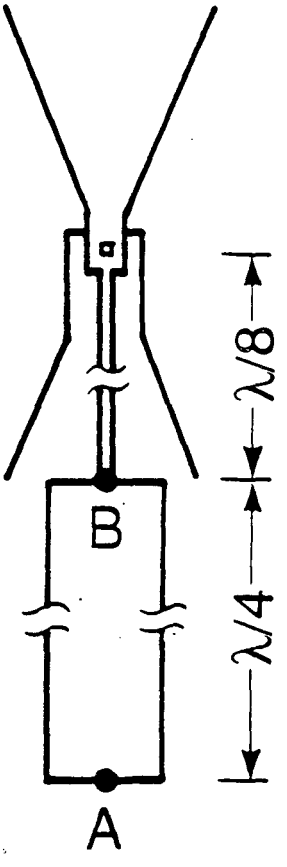

(b)

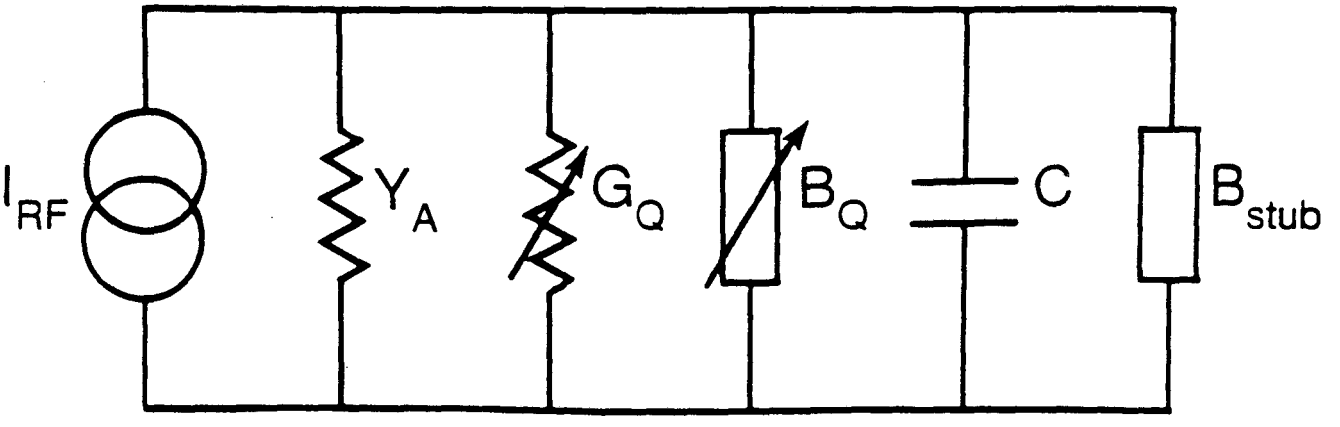

(c)

Figure 2

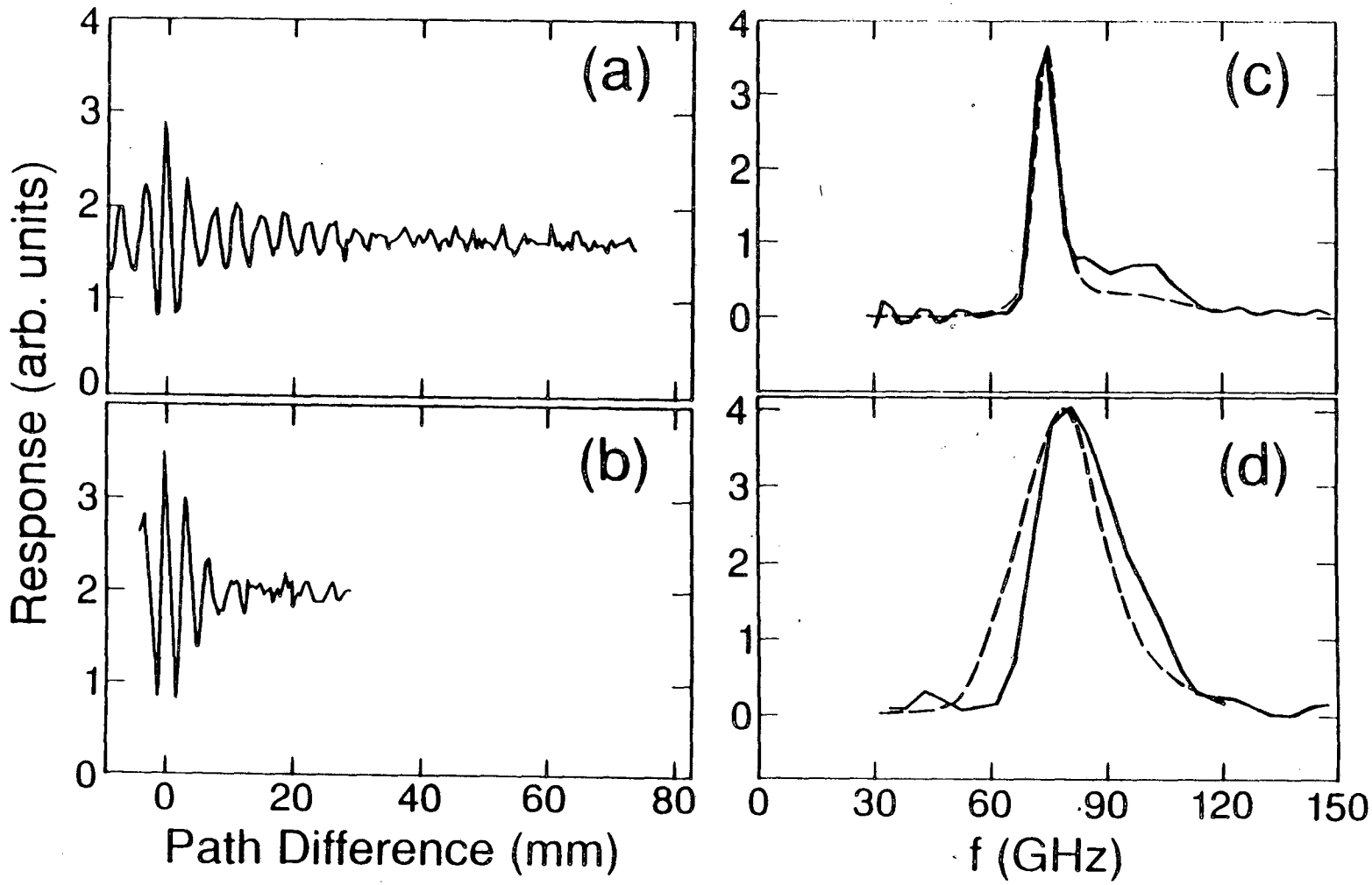
Response (arb. units)
(a)
(b)
(c)
(d)
0
1
2
3
4
0
20
40
60
80
Path Difference (mm)
0
30
60
90
120
150
f (GHz)

Figure 3

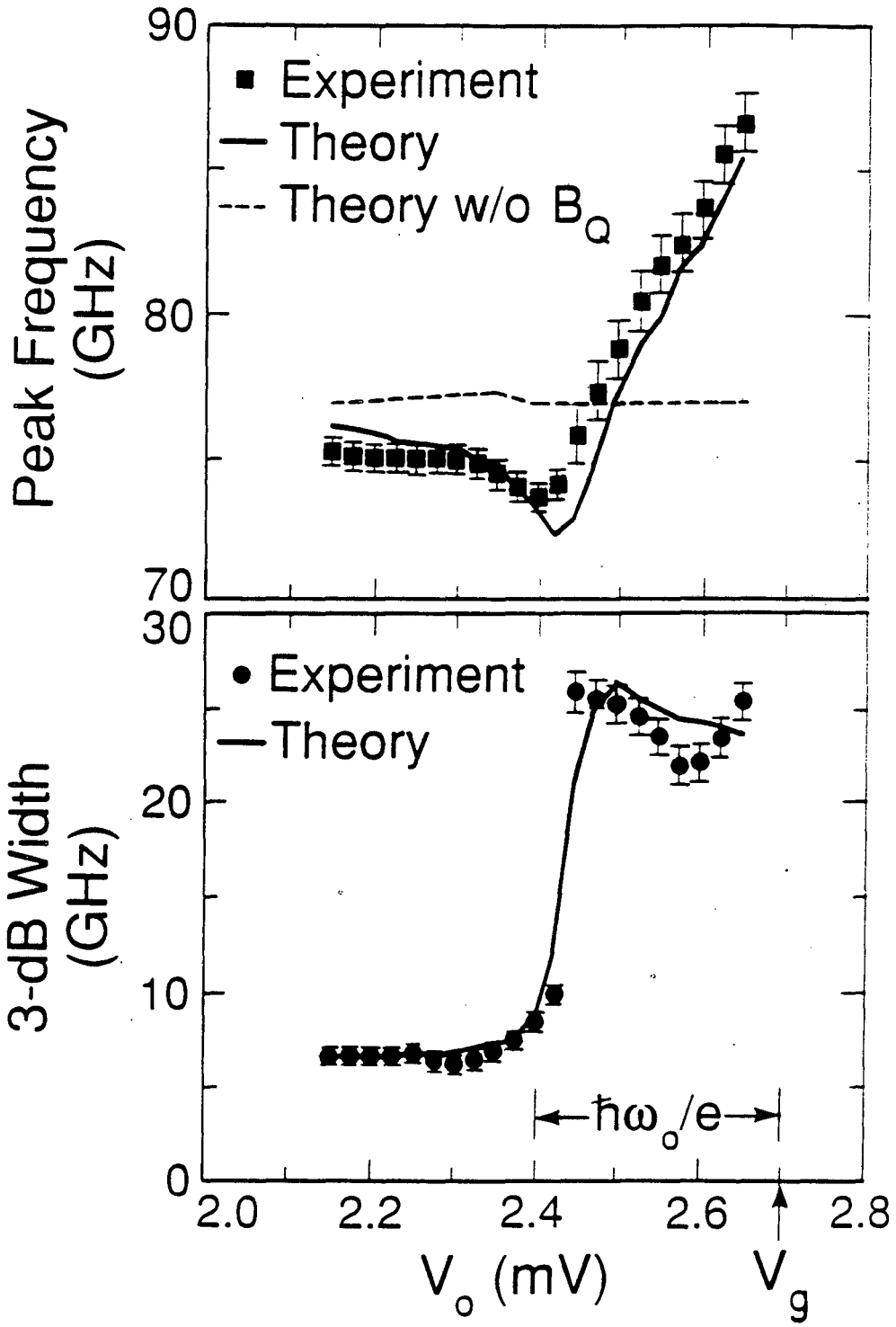
90
80
70
Peak Frequency (GHz)
Experiment
Theory
Theory w/o B_Q
30
20
10
0
3-dB Width (GHz)
Experiment
Theory
$\hbar\omega_o/e$
2.0
2.2
2.4
2.6
2.8
V_o (mV)
V_g

Figure 4

LAWRENCE BERKELEY LABORATORY
TECHNICAL INFORMATION DEPARTMENT
1 CYCLOTRON ROAD
BERKELEY, CALIFORNIA 94720